Large-scale magnetic field generation via the Kelvin-Helmholtz instability

E. P. Alves[1], T. Grismayer[1]

S. F. Martins[1], F. Fiúza[1], R. A. Fonseca[1,2], L. O. Silva[1]

ABSTRACT

We present the first self-consistent three-dimensional particle-in-cell simulations of the Kelvin-Helmholtz instability (KHI) in an unmagnetized scenario. We discuss the main features, including density structure formation, and magnetic field generation, its evolution and saturation on the electron time-scale. The linear theory of the longitudinal KHI dynamics is presented, including arbitrary density jumps between shearing flows, showing that the onset of the instability is robust to this asymmetry. Simulations provide new insights into the evolution of the KHI in three dimensions, revealing the formation of complex structures due to the transverse dynamics of the instability and the emergence of a strong and large-scale DC magnetic field component which is not captured by the standard linear fluid theory. Our results indicate that the KHI can generate magnetic fields up to $\epsilon_B/\epsilon_p \simeq 10^{-3}$ in the electron time-scale.

Subject headings: magnetic field generation – plasma instabilities – Kelvin-Helmholtz instability

1. Introduction

Magnetic field generation in extreme astrophysical scenarios, such as active galactic nuclei (AGN) and gamma-ray bursts (GRBs), is not fully understood (Colgate 2001). While such phenomena are of fundamental interest, they are also closely related to open questions like processes of non-thermal radiation and cosmic ray production (Bhattacharjee 2000). Recently, collisionless plasma effects have been proposed as candidate mechanisms for magnetic field generation (Gruzinov & Waxman 1999; Medvedev & Loeb 1999) as, for instance,

[1]GoLP/Instituto de Plasmas e Fusão Nuclear - Laboratório Associado, Instituto Superior Técnico, Lisbon, Portugal

[2]Instituto Universitário de Lisboa (ISCTE-IUL), Lisbon, Portugal

the Weibel (Weibel 1959; Silva et al. 2003) and Kelvin-Helmholtz (KH) (D'Angelo 1965; Gruzinov 2008; Zhang et al. 2009) instabilities. The KHI is an important candidate, capable of generating magnetic fields in the presence of strong velocity shears which may naturally originate in energetic matter outbursts of AGN and GRBs. These fields may then be further amplified by the magnetic-dynamo effect (Gruzinov 2008; Zhang et al. 2009).

Recent numerical kinetic simulations have aimed at magnetic field generation via electromagnetic plasma instabilities in unmagnetized flows without velocity shears. Three-dimensional (3D) particle-in-cell (PIC) simulations of Weibel turbulence are presented in (Silva et al. 2003; Fonseca et al. 2003; Frederiksen 2004; Nishikawa 2005), demonstrating magnetic field generation. It has been reported that the Weibel instability can mediate relativistic shocks (Spitkovsky 2008; Martins et al. 2009) where a Fermi-like particle acceleration process is observed. Other collisionless plasma instabilities have been examined in different system settings, in particular, with velocity shears as an alternative mechanism to generate sub-equipartition magnetic fields in relativistic outflows (Gruzinov 2008). In Zhang et al. (2009), a 3D magnetohydrodynamic (MHD) simulation of KH turbulence is discussed, observing magnetic field amplification due to KH-induced turbulent dynamo. However, a 3D fully kinetic PIC simulation of the KHI in unmagnetized plasma remains lacking. Moreover, recent laboratory astrophysics experiments have focused on the development of the KHI in collisionally dominated high energy-density plasmas (Harding 2009).

In this Letter, we present the first self-consistent 3D PIC simulations of the KHI for both subrelativistic and relativistic scenarios of shearing, unmagnetized electron-proton plasma clouds. We focus on the physical processes underlying magnetic field amplification from thermal fluctuations, and electron density structure formation. In addition to the longitudinal Kelvin-Helmholtz vortices, we observe transverse modulations which are not captured in previous 3D MHD simulations (Zhang et al. 2009). Furthermore, we generalize the KHI linear theory (Gruzinov 2008) to include arbitrary density jumps between the shearing flows, and conclude that the onset of the instability is robust to this asymmetry. The analytical results are compared with numerical simulations. Our simulations also demonstrate the generation of a DC magnetic field which can only be captured in kinetic simulations due to the plasma heating in the development of the KHI.

This paper is organized as follows: in Section 2, we extend the existing linear fluid theory of the KHI to include arbitrary density jumps, and examine this effect on the behavior and features of the instability. The theoretical growth rates, fastest growing modes, and their dependence on the density ratio between shearing flows agree with the numerical simulations. In Section 3, we present and discuss the results of the 3D PIC simulations in detail. Conclusions are drawn in Section 4.
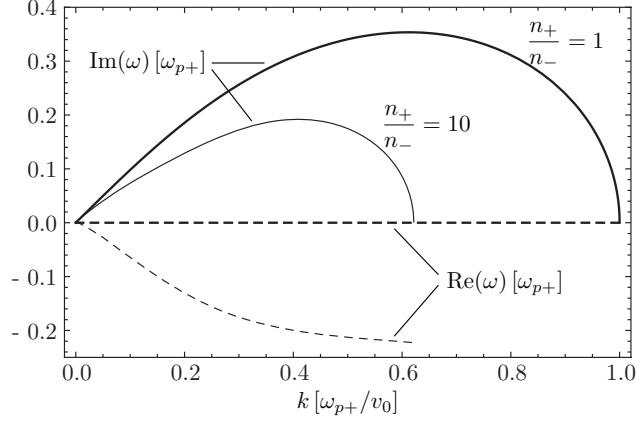
2. Theoretical analysis

Fig. 1.— Real (dashed curves) and imaginary (solid curves) parts of ω' for the symmetric $(n_+/n_- = 1)$ and an asymmetric $(n_+/n_- = 10)$ density regimes. The density symmetric and asymmetric regimes are represented by the blue and red curves, respectively.

The theoretical model describing the linear development of the KHI, outlined in Gruzinov (2008), is based on the relativistic fluid formalism of plasmas coupled with Maxwell's equations, and was analyzed for the special case where the two shearing flows have the same density. Realistic shears, however, are more likely to occur between different density flows.

We have extended the analysis presented in Gruzinov (2008) for shearing electron-proton plasma flows with uniform number densities n_+ and n_-, and counter-propagating velocities $+\vec{v}_0$ and $-\vec{v}_0$, respectively. Here, the protons are considered free-streaming whereas the electrons are linearly perturbed. Considering these density and velocity profiles into the linearized relativistic fluid plasma equations, one arrives at the following dispersion relation for electromagnetic waves:

$$\sqrt{\frac{n_-}{n_+} + \frac{k'^2}{\beta_0^2} - \omega'^2} \left[\left(\omega' + k'\right)^2 - \left(\omega'^2 - k'^2\right)^2 \right] +$$

$$\sqrt{1 + \frac{k'^2}{\beta_0^2} - \omega'^2} \left[\frac{n_-}{n_+} \left(\omega' - k'\right)^2 - \left(\omega'^2 - k'^2\right)^2 \right] = 0,$$

where $\omega' \equiv \omega/\omega_{p+}$ is the wave frequency normalized to the plasma frequency, with number density n_+, $\omega_{p+} = (n_+ e^2/\epsilon_0 \gamma_0^3 m_e)^{1/2}$. $k' \equiv k v_0 c/\omega_{p+}$ is the normalized wave number, $\beta_0 = v_0/c$ and $\gamma_0 = (1 - \beta_0^2)^{-1/2}$ is the Lorentz relativistic factor; e and m_e are the electron charge and mass, respectively, ϵ_0 is the electric permittivity of vacuum, and c is the speed of light in vacuum.

The density contrast feature is included in the dispersion relation through the density ratio n_+/n_-. In the same-density scenario, $n_+/n_- = 1$, the modes with $|k'| < 1$ are unstable, with a maximum growth rate $\Gamma'_{\max} = \Gamma_{\max}/\omega_{p+} = 1/\sqrt{8}$ for the fastest growing mode $k'_{\max} = k_{\max}v_0/\omega_{p+} = \sqrt{3/8}$. The real part of ω' vanishes over the range of unstable modes, meaning that the unstable modes are purely growing waves. On the other hand, in the density-contrast scenario, $n_+/n_- \neq 1$, the shape of the spectrum is conserved for different density ratios, indicating that the general characteristics of the instability are unchanged. As n_+/n_- increases, the bandwidth of unstable modes decreases, $k'_{\max}$ drifts to larger scales, and the growth rate $\Gamma'_{\max}$ decreases. Furthermore, the frequency, ω', acquires a real part over the range of the unstable modes, indicating that the growing perturbations propagate. The density-contrast unbalances the interaction between flows such that the growing perturbations are more strongly manifested in the less dense flow, and drift in the direction of this less dense flow. In the same-density case, the interaction between flows is balanced and the perturbations do not drift.

The normalized growth rate of the fastest growing mode, $\Gamma'_{\max}$, decreases with the density ratio between flows. In the similar density regime, $n_+/n_- \approx 1$, the growth rate scales approximately as $\Gamma'_{\max} \propto (n_+/n_-)^{-1/4}$ for both relativistic and non-relativistic shears. In the high density contrast regime, $n_+/n_- \gg 1$, the growth rate scales as $\Gamma'_{\max} \propto (n_+/n_-)^{-1/3}$ for non-relativistic shears (similar to the small cold beam-plasma instability, (?)), and $\Gamma'_{\max} \propto (n_+/n_-)^{-1/2}$ for highly-relativistic shears.

The theoretical predictions on the density contrast effect show good agreement with both 2D and 3D PIC simulations. A further detailed analysis of the theoretical model and its comparison with simulations will be presented in a separate publication (E. P. Alves 2011, in preparation).

3.   3D PIC simulations

Numerical simulations were performed with OSIRIS, a fully relativistic, electromagnetic, and massively parallel PIC code (Fonseca et al. 2003, 2008).

We simulate 3D systems of shearing slabs of cold ($v_0 \gg v_{th}$, where v_{th} is the thermal velocity) unmagnetized electron-proton plasmas with a realistic mass ratio $m_p/m_e = 1836$ (m_p is the proton mass), and evolve it until the electromagnetic energy saturates on the electron time scale. In this Letter, we explore a subrelativistic ($\gamma_0 = 1.02$) and a relativistic ($\gamma_0 = 3$) KHI scenario. The numerical simulations are prepared as follows. The shear flow initial condition is set by a velocity field with v_0 pointing in the positive x_1 direction, in the

upper and lower quarters of the simulation box, and a symmetric velocity field with $-v_0$ pointing in the negative x_1 direction, in the middle-half of the box. Initially, the systems are charge and current neutral, and the shearing flows have equal densities. In the subrelativistic case, the simulation box dimensions are $20 \times 20 \times 20 \ (c/\omega_p)^3$, where $\omega_p = (ne^2/\epsilon_0 m_e)^{1/2}$ is the plasma frequency, and we use 20 cells per electron skin depth (c/ω_p). The simulation box dimensions for the relativistic scenario are $250 \times 80 \times 80 \ (c/\omega_p)^3$, with a resolution of 4 cells per c/ω_p. Periodic boundary conditions are imposed in every direction. In order to ensure result convergence, higher numerical resolutions and more particles per cell were tested.

The magnetic field structures generated in the subrelativistic and relativistic shear scenarios are displayed in Figures 2 and 3, respectively. In the linear regime, the onset of the fluid KHI, discussed in Section 2, occurs in the $x_1 x_3$ plane around the shear surfaces, generating a magnetic field normal to this plane, B_2. The typical length scale of the KHI modulations, observed in Figures 2 f and 3 f, agrees with the wavelength of the most unstable mode predicted by the fluid theory in Section 2 ($\lambda_{\mathrm{max}} = 2 \ c/\omega_p$ in the subrelativistic case, and $\lambda_{\mathrm{max}} \simeq 50 \ c/\omega_p$ in the relativistic case). The KHI modulations, however, are less noticeable in the relativistic regime because these are masked by a strong DC component ($k_{x_1} = 0$ mode), with a magnitude higher than the AC component, which is negligible in the subrelativistic regime. This DC magnetic field, is not unstable according to the fluid model (Figure 1), and results from intrinsically kinetic phenomena. As the amplitude of the KHI modulations grow, the electrons from one flow cross the shear surfaces and enter the counter-streaming flow. Since the protons are unperturbed, due to their inertia, the current neutrality around the shear surfaces is unbalanced, forming DC current sheets, which point in the direction of the proton velocity. These DC current sheets induce a DC component in the magnetic field B_2. The DC magnetic field is therefore dominant in the relativistic scenario since a higher DC current is setup by the crossing of electrons with a larger initial flow velocity, compared with the subrelativistic case. The growing magnetic field component B_2 is responsible for rolling-up the electrons to form the signature KH vortices (insets a2 and b2 of Figure 4) while further slowing down the electrons along x_1 and enhancing the shear-surface current sheets in a feedback loop process. This mechanism underlies the growth of B_2 as illustrated in Figure 4, which shows the evolution of the magnetic field energy divided into its components for both subrelativistic and relativistic scenarios.

Novel electron density structures, which have not been reported in MHD simulations to our knowledge (Keppens 1999; Zhang et al. 2009), emerge in the plane transverse to the flow direction (insets a1 and b1 of Figure 4), and extend along the x_1 direction forming electron current filaments. A harmonic perturbation in the B_3 component of the magnetic field at the shear surfaces forces the electrons to bunch at the shear planes forming current filaments, which amplify the initial magnetic perturbation B_3. This process is identical to the

one underlying the Weibel instability (Medvedev & Loeb 1999) and leads to the formation of the observed transverse current filaments, along with the exponential amplification of B_3 observed in Figure 4. Figures 2 g and 3 g further show that the B_3 magnetic field component shares a filamentary structure, underlining its role in this process. Note that in spite of the absence of bulk interpenetration between flows, which is known to drive the Weibel, this setup of counter-streaming plasma clouds interacting at a shear surface provides sufficient conditions for this Weibel-like mechanism to operate. Meanwhile, electrons undergoing the bunching process slow down along their initial flow direction. Again, since the protons are unperturbed at these time-scales, DC ($k_{x_2} = 0$ mode) current sheets are setup around the shear surfaces in a similar fashion to the longitudinal dynamics. These current sheets induce a DC magnetic field in B_2, which is shown in Figures 2 e and 3 e. This magnetic field is responsible for accelerating the evolving filaments across the shear surface, into the counter-propagating flow. In the relativistic shear scenario, these filaments are strongly rotated due to the high intensity of B_2, into the opposing flow, leading to the formation of well defined finger-like density structures, as seen in inset b1 of Figure 4. These structures are less pronounced in the subrelativistic shear scenario due to the lower intensity of the DC component of B_2 and to the slower Weibel-like electron bunching process (inset a1 of Figure 4). Meanwhile, the current density component J_3 arises from the crossing motion of the current filaments along the x_3 direction, inducing the magnetic field component B_1. The regions of B_1 are observed in inset b of Figures 2 and 3 to be found between counter-streaming electron filaments. A more thorough discussion on the transverse dynamics of the KHI will be presented in a separate publication (E. P. Alves 2011, in preparation).

The growth rate of the magnetic field in the subrelativistic regime matches the theoretical growth rate of the fastest growing mode $\Gamma_{max} = 0.35 \ \omega_p$ (Figure 4 a). 2D simulations matching the longitudinal (x_1x_3) and transverse (x_2x_3) planes of the 3D subrelativistic setup were performed to assess the independent evolution of both the longitudinal and transverse dynamics of the KHI. We observed that the growth rate of the transverse dynamics ($\Gamma^{2D}_{transverse} \simeq 0.1 \ \omega_p$) is much lower than the growth rate of the longitudinal dynamics ($\Gamma^{2D}_{longitudinal} \simeq 0.35 \ \omega_p$), which reproduces the 3D growth rate. The longitudinal dynamics is therefore dominant over the transverse dynamics in the linear regime of the subrelativistic scenario. In contrast, we measure a growth rate of $\simeq 0.3 \ \omega_p$ in the relativistic scenario (Figure 4 b), which is much higher than the theoretical growth rate of the fastest growing mode of the longitudinal dynamics, $\Gamma_{max} = 0.07 \ \omega_p$. The results of matching 2D simulations of the 3D relativistic setup, however, revealed a growth rate of $\Gamma^{2D}_{transverse} \simeq 0.3 \ \omega_p$ for the transverse dynamics, and $\Gamma^{2D}_{longitudinal} \simeq 0.07 \ \omega_p$ for the longitudinal dynamics, thus indicating that the growth of the magnetic fields in the linear regime of the 3D relativistic scenario is mainly determined by the transverse dynamics of the KHI.

At later times, the growing longitudinal and transverse KH electron density structures begin to interact with each other and merge, ultimately guiding the system into a turbulent state. Eventually, all large-scale shear surfaces in the electron structure become extinct, inhibiting the operation of the electron-scale KHI, and the instability saturates. This stage is reached at roughly $t \simeq 100/\omega_p$ in both subrelativistic and relativistic scenarios. In this turbulent state, the drift velocity of the electrons vanishes and the magnetic field is mainly sustained by the proton current sheets around the shear-surfaces. Here, most of the magnetic field energy is deposited in B_2, revealing a uniform DC structure at the shear-surfaces with a characteristic transverse thickness L_{sat}. The AC modulations in the magnetic field structure are at this time negligible compared with the DC component. This uniform magnetic field structure is rather relevant since it extends along the length and width of the shear-surface, which may be extremely large-scale in realistic astrophysical shears. Using Faraday's equation and neglecting the displacement current term, we may estimate the amplitude of the magnetic field as $B_{\text{DC}} \sim e\mu_0 n_0 v_0 L_{\text{sat}}/2$, where μ_0 is the magnetic permeability of vacuum. This estimate agrees with the simulation results and can be used to determine the average equipartition value ϵ_B/ϵ_p (ratio of magnetic to initial particle kinetic energy) of the system as

$$\frac{\epsilon_B}{\epsilon_p} \sim \frac{1}{8}\frac{m_e}{m_p}\frac{\gamma_0+1}{\gamma_0^2}\frac{L_{\text{sat}}^3}{L_{x_2}}\frac{\omega_p^2}{c^2},$$

where $\epsilon_p = n_0(m_p+m_e)c^2(\gamma_0-1)L_{x_1}L_{x_2}L_{x_3}$ (L_{x_i} being the simulation box dimension in the x_i direction). We measure from the simulation at saturation $L_{\text{sat}} \simeq 4\, c/\omega_p$ for the subrelativistic case and $L_{\text{sat}} = 15\, c/\omega_p$ for relativistic case. The estimates of the equipartition values are thus 4×10^{-4} for the subrelativistic and 1.2×10^{-3} for the relativistic scenarios, respectively, which are comparable with the simulations results of 2×10^{-4} and 8×10^{-4} (Figure 4). We may also estimate the maximum value of equipartition which is found at the shear surfaces as,

$$\frac{\epsilon_B}{\epsilon_p} \sim \frac{1}{8}\frac{m_e}{m_p}\frac{\gamma_0+1}{\gamma_0^2}L_{\text{sat}}^2\frac{\omega_p^2}{c^2},$$

yielding 2×10^{-3} for the subrelativistic case and 7×10^{-3} for the relativistic case. A higher efficiency of conversion of particle kinetic energy to magnetic fields is observed in the relativistic case since the thickness of the proton currents sheets (L_{sat}) is much higher than in the subrelativistic case. Most of the energy in the system, however, is still contained in the ions which remain unperturbed at these time-scales. We expect the system to reach higher levels of equipartition once the protons undergo the proton-scale KHI, which would occur at roughly $t_{\text{proton−KHI}} \simeq 100\, (mi/me)^{1/2}/\omega_p \simeq 4000/\omega_p$.

4. Conclusions

In this Letter, we present the first self-consistent 3D PIC simulations of KH unstable scenarios and analyze their evolution on the electron time-scale. We mainly focus on the physical processes underlying electron density structure formation and magnetic field generation. The linear development of the longitudinal KHI dynamics reveals good agreement with the 2D theoretical model, namely growth rates and typical length-scales of the emerging structures. We also observe the appearance of a DC component in the magnetic field at the shear surfaces, which is not captured by the fluid theory.

Furthermore, numerical simulations reveal structure formation transverse to the KH vortices, demonstrating the transverse features of the KHI. Electron current filaments evolve at the shear-surfaces in the transverse direction to the flows due to a Weibel-like electron-bunching process. These filaments are then accelerated across the shear surfaces forming finger-like electron density structures. In relativistic shear scenarios, the evolution of the KHI is mainly determined by the transverse dynamics, whereas the longitudinal dynamics is dominant in subrelativistic shears. At the electron saturation time-scale the magnetic field has evolved to a large-scale DC field structure at the shear surfaces, formed by non-linear merging of the magnetized clumps which were generated at the early stages of the KHI. We measure maximum equipartition values of $\epsilon_B/\epsilon_p \simeq 2 \times 10^{-3}$ for the subrelativistic scenario, and $\epsilon_B/\epsilon_p \simeq 7 \times 10^{-3}$ for the relativistic scenario, which agree with our estimates, implying that the majority of the magnetic field energy is contained in the DC component. Moreover, the onset of the KHI is robust to density asymmetries making it ubiquitous in astrophysical settings. The equal density regime, $n_+/n_- \approx 1$, is relevant in internal shocks, where shearing occurs between identical flows, contrasting to the high-density-jump regime, $n_+/n_- \gg 1$, which is important in external shocks, where shearing may arise between the ejecta and the interstellar medium, for example.

In summary, our results show that the multidimensional physics of the KHI is extremely rich and that kinetic effects play an important role, in particular, in the generation of a strong large scale DC magnetic field. The DC magnetic field extends over the entire shear-surface, reaching thicknesses of a few tens of electron skin depths, and persists on time-scales much longer than the electron time scale. The generation of large-scale magnetic fields by the KHI can play a crucial role in non-thermal radiation emission processes and particle acceleration in astrophysical scenarios.

REFERENCES

Colgate S. A., Li H., Pariev V., 2001, Phys. Plasmas, 8, 2425

Bhattacharjee P. & Sigl G. 2000, Phys. Rep.-Rev Sec. of Phys Lett, 327, 109

Weibel E. S. 1959, Phys. Rev. Lett., 2, 83

D'Angelo N. 1965, Phys. Fluids, 8, 1748

Harding E. C. et al. 2009, Phys. Rev. Lett., 203

Kuranz C. C. et al. 2009, ApJ, 696, 749

Foster J. M. et al. 2005, ApJ, 634, L77

Gruzinov A. 2008, arXiv:0803.1182

O'Neil T. M., Winfrey J. H., Malmberg J. H. 1971, Phys. Fluids, 14, 1204

Silva L. O., Fonseca R. A., Tonge J. W., Dawson J. M., Mori W. B., & Medvedev M. V. 2003, ApJ, 596, L121

Fonseca R. A., Silva L. O., Tonge J. W., Mori W. B., & Dawson J. M. 2003, Phys. Plasmas, 10, 1979

Fonseca R. A. et al. 2008, Phys. Plasmas and Controlled Fusion, 50, 12

Martins S. F., Fonseca R. A., Silva L. O., & Mori W. B. 2009, ApJ, 695, L189

Gruzinov A. & Waxman E. 1999, ApJ, 511, 852

Zhang W., MacFadyen A., & Wang P. 2009, ApJ, 692, L40

Spitkovsky A. 2008, ApJ, 682, L5

Medvedev M. V. & Loeb A. 1999, ApJ, 526, 697

Keppens R., Toth G., Westermann R. H. J., Goedbloed J. P., 1999, Journal of Plasma Physics, 61

Frederiksen J. T. et al. 2004, ApJ, 608, L13

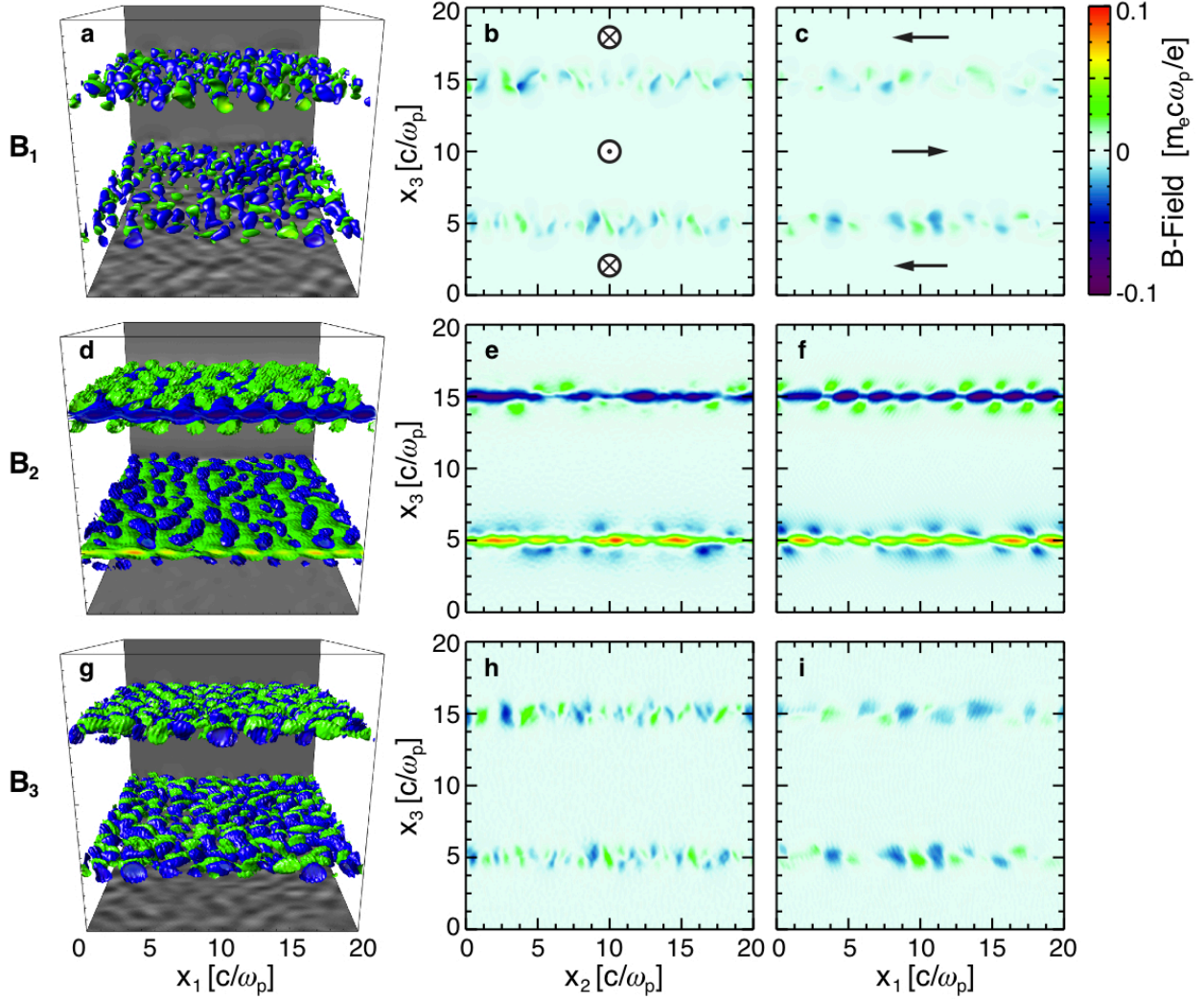Nishikawa K.-I. et al. 2005, ApJ, 622, 927

Fig. 2.— Magnetic field structures generated by shearing subrelativistic e^-p^+ flows with $\gamma_0 = 1.02$ taken at time $t = 49/\omega_p$. The three-dimensional visualizations (a), (d) and (g) correspond to the magnetic field components B_1, B_2 and B_3, respectively. The two-dimensional slices of the magnetic field intensity (b), (e) and (h) are taken at the centre of the box $x_1 = 10 \ c/\omega_p$, and slices (c), (f) and (i) are taken at $x_2 = 10 \ c/\omega_p$.
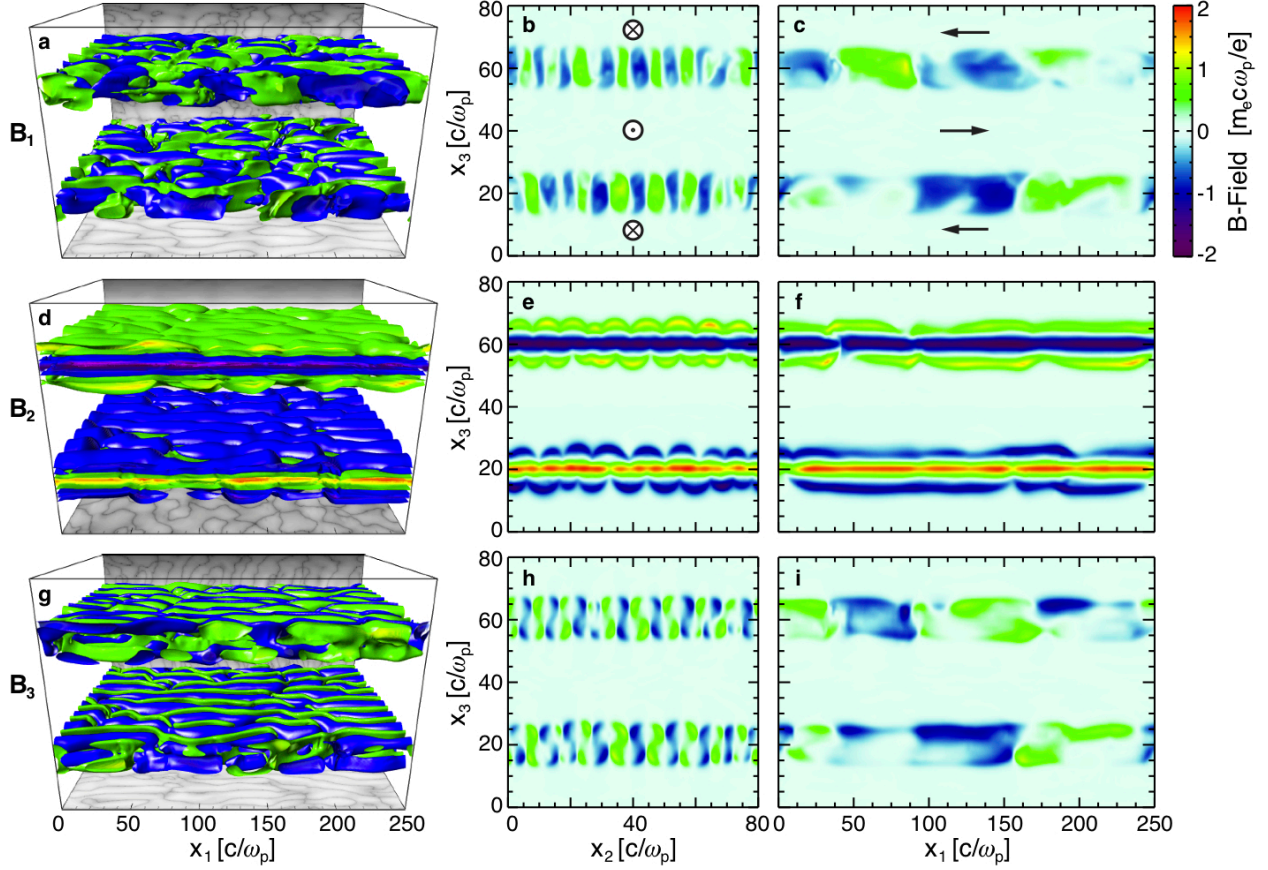
Fig. 3.— Magnetic field structures generated by shearing relativistic e^-p^+ flows with $\gamma_0 = 3$ taken at time $t = 69/\omega_p$. The three-dimensional visualizations (a), (d) and (g) correspond to the magnetic field components B_1, B_2 and B_3, respectively. The two-dimensional slices of the magnetic field intensity (b), (e) and (h) are taken at the centre of the box $x_1 = 125\ c/\omega_p$, and slices (c), (f) and (i) are taken at $x_2 = 40\ c/\omega_p$.
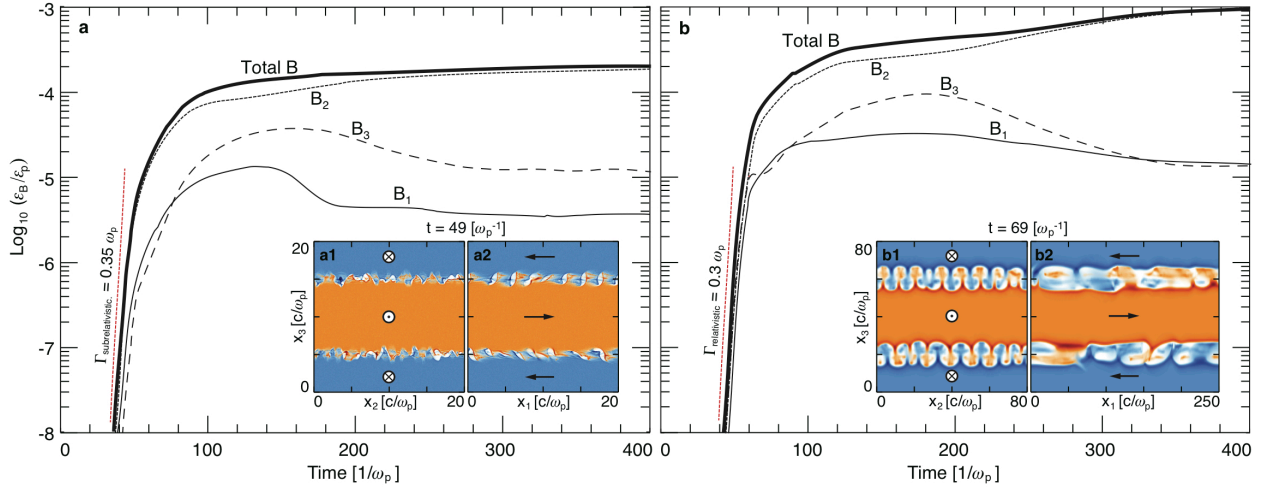
Fig. 4.— Evolution of the equipartition energy ϵ_B/ϵ_p for a (a) subrelativistic and (b) relativistic shear scenarios. The contribution of each magnetic field component is also depicted. The insets in each frame represent two-dimensional slices of the electron density at $t = 49/\omega_p$ and $t = 69/\omega_p$ for the respective case. The red (blue) color represents the electron density of the plasma that flows in the positive (negative) x_1 direction. Darker regions in the colormap mean high electron density, whereas lighter regions mean low electron density. Slices for insets (a1), (a2), (b1) and (b2) were taken at the center of the simulation box; (a1) and (b1) are transverse to the flow direction, and slices (a2) and (b2) are longitudinal to the flow direction.